ACS APPLIED MATERIALS & INTERFACES

Research Article

Cite This: ACS Appl. Mater. Interfaces 2017, 9, 44715−44723

www.acsami.org

Graphene/PbS-Quantum Dots/Graphene Sandwich Structures Enabled by Laser Shock Imprinting for High Performance Photodetectors

Qiong Nian,[†,‡] Liang Gao,[§] Yaowu Hu,[†,‡] Biwei Deng,[†,‡] Jiang Tang,*[,§] and Gary J. Cheng*[,†,‡]

[†]School of Industrial Engineering, Purdue University, West Lafayette, Indiana 47906, United States

[‡]Birck Nanotechnology Center, Purdue University, West Lafayette, Indiana 47906, United States

[§]Wuhan National Laboratory for Optoelectronics, Huazhong University of Science and Technology (HUST), Wuhan 430074, China

ABSTRACT: Quantum dots (QDs) integrated 2-dimensional (2D) materials have great potential for photodetector applications due to the excellent light absorption of QDs and ultrafast carrier transportation of 2D materials. However, there is a main issue that prevents efficient carrier transportation and ideal performance of photodetectors: the high interfacial resistance between 2D materials and QDs due to the bad contacts between 2D/0D interface, which makes sluggish carrier transfer from QDs to 2D materials. Here, a sandwich structure (graphene/PbS-QDs/graphene) with seamless 2D/0D contact was fabricated by laser shock imprinting, which opto-mechanically tunes the morphology of 2D materials to perfectly wrap on 0D materials and efficiently collect carriers from the PbS-QDs. It is found that this seamless integrated 2D/0D/2D structure significantly enhanced the carrier transmission, photoresponse gain (by 2×), response time (by 20×), and photoresponse speed (by 13×). The response time (~30 ms) and I_p/I_d ratio (13.2) are both over 10× better than the reported hybrid graphene photodetectors. This is due to the tight contact and efficient gate-modulated carrier injection from PbS-QDs to graphene. The gate voltage dictates whether electrons or holes dominate the carrier injection from PbS-QDs to graphene.

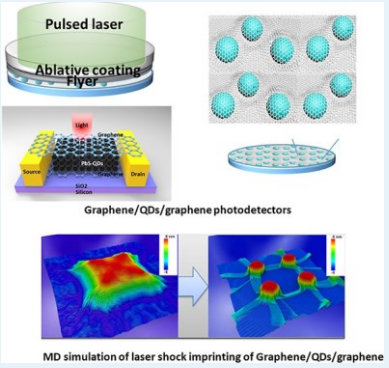

KEYWORDS: microfabrication, photodetector, quantum dot, graphene, response time, photoresponse rate, photoresponse gain

INTRODUCTION

Interface engineering performs important roles in two-dimensional (2D) materials transportation[1,2] and device fabrication.[3,4] Although interface measurement[5−7] has been mature for decades, rare interface modification method has been investigated. Graphene, as a 2D material, draws plenty of attention due to its flat monolayer of carbon atoms exhibiting ultrahigh strength and free carrier mobility.[8] In spite of this, graphene shows limitations such as weak light absorption,[9] contact induced defects,[10] and the lack of bandgap.[11] Thus, graphene hybrid structures rather than pristine graphene were primarily studied in functional devices, including photodetectors,[12] electronics,[10] capacitors,[13] solar cells,[14] etc. The combination of QDs and graphene take full advantage of the tunable and strong light absorption of QDs and the high conductivity of graphene, thereby makes the hybrid graphene/ QDs dots photodetector to achieve ultrahigh responsivity.[15−17] Ultrasensitive graphene/PbS-QDs based infrared photodetector,[16] which is vitally useful in temperature detection in industry, has also been intensely studied. However, exfoliated graphene and toxigenic chemicals used during the fabrication make the photodetector either too complicated or too dangerous to be practically implemented. Although CVD graphene[15] has been successfully used in infrared photodetector fabrication, only one single layer graphene served as carriers

channel at the bottom could not efficiently collect all the photogenerate carries. Here, we present a graphene/PbS-QDs/ graphene hybrid photodetector, where two graphene layers perform as two carrier channels. However, traditional graphene transfer method[18] limits the contact between top layer graphene and underlying 3D surface to grid-space contact rather than perfectly wrapping contact, resulting in a weak transportation between graphene and the underlying materials and unavoidable artificial scattering centers. Laser shock imprinting[19] is a technique to utilize laser to generate plasma gas in a confined volume that can induce GPa scale pressure to generate nanopatterning in various materials. Previously, this method was proven to be able to deform metals[20] and nanowires[21] into different nanopatterns depending on the morphology of the underlying substrate. In this work, we take advantage of laser shock imprinting to generate nanoscale wrapping of graphene on QDs and

DOI: 10.1021/acsami.7b14468
ACS Appl. Mater. Interfaces 2017, 11, 44715−44723

improve the interface between graphene and PbS-QDs from grid-space contact to perfect 3D integration. Our results suggest such changes could dramatically increase transmission, photoresponse gain, and photoresponse speed.

Received: September 24, 2017
Accepted: December 4, 2017
Published: December 4, 2017

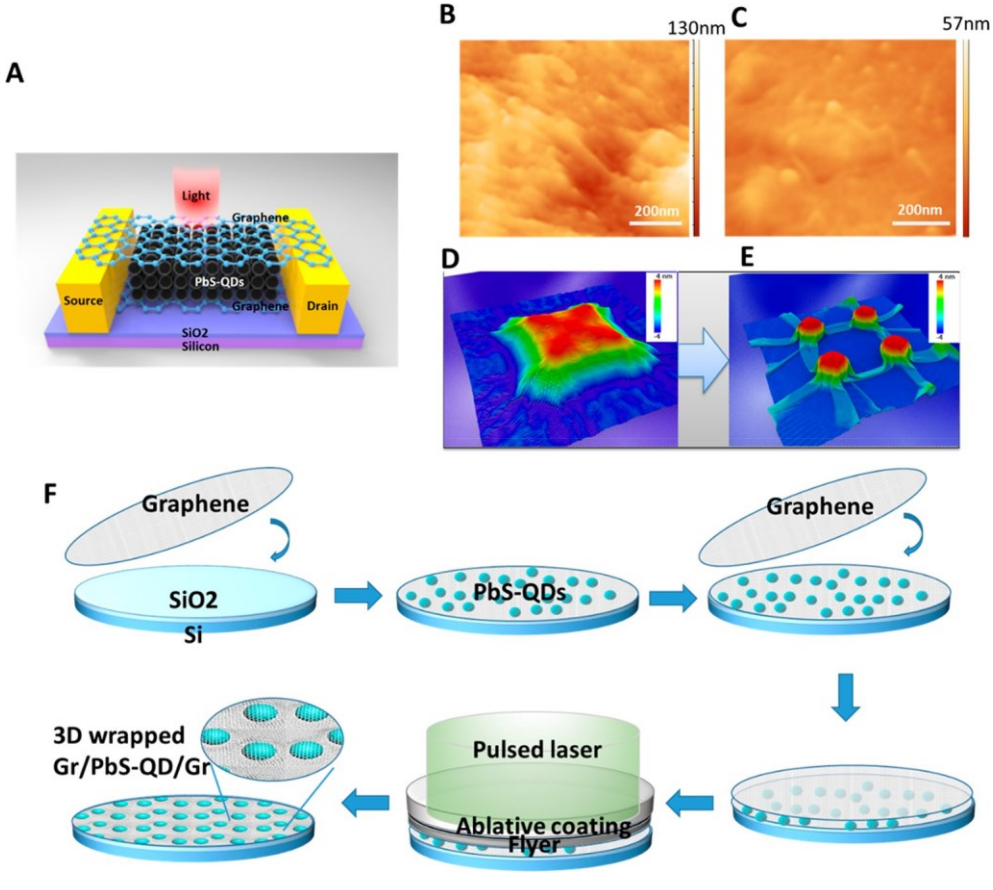

Figure 1. Hybrid graphene/PbS-QDs/graphene photodetectors. (A) Structure of graphene/PbS/graphene hybrid structures. The channel length between source and drain is 50 μm. AFM image of graphene wrapped on PbS QDs (B) before and (C) after laser shock fabrication. MD simulation results demonstrate graphene wrapping on 3D feature surface (D) before and (E) after the laser shock process. (F) Fabrication flow of the laser shock imprinting enabled graphene/PbS-QDs/graphene seamless hybrid structure.

RESULTS AND DISCUSSION

Well-Defined and Seamless Integrated 2D/0D/2D Structure. Herein, we design and fabricate a sandwichstructured graphene/PbS-QDs/graphene photodetector as shown in Figure 1A. The bottom graphene layer was transferred onto a bottom gate SiO_2/Si substrate. A 60 nmthick PbS-QDs film was coated as the photoresponse layer, and finally the top graphene layer was transferred onto PbS-QDs film, followed by laser shock imprinting. Au−Ti electrode was thermally evaporated as source and drain of the sensor. The two graphene layers (bottom and top) serve as two carrier channels that are able to collect photogenerated carriers from PbS-QDs.[22] The light beam would pass through top layer graphene and be absorbed by PbS-QDs to excite electron−hole pairs. These photogenerated carriers, which would be injected into both graphene layers on top and bottom, could both contribute to the photoresponse. The merits of such a device is that the top layer graphene would serve as an extra channel for carrier transportation, and high carrier mobility of graphene on the top would dominate the shortcoming of 2.3% light blocking.[9,23] However, the morphology of graphene on the top of PbS-QDs could make a big influence. This sandwichstructured device was processed by laser shock imprinting, and the corresponding structure change was investigated before and after. Figures 1B and C display laser shock effect for graphene wrapped on PbS-QDs, in which the surface morphology was characterized by atomic force microscopy (AFM). Wet transferred graphene only covered loosely or was suspended on PbS-QDs surface; thus, a rugged surface with ups-anddowns was detected (Figure 1B). On the contrary, after laser shock, the loosely covered graphene was punched onto the 3D surface of PbS QDs, resulting in the super smooth surface just like PbS-QDs only, as if the graphene never existed (Figure 1C). This also was demonstrated by the surface roughness decrease from 130 to 57 nm after the laser shock process. The laser shock

DOI: 10.1021/acsami.7b14468
ACS Appl. Mater. Interfaces 2017, 11, 44715−44723

wrapping effects are also consistent with the MD simulation results in Figures 1D and E, in that the suspended graphene is seamlessly wrapped on QDs after laser shock imprinting. The details of the simulation and physical mechanism of laser shock imprinting are discussed later in this report. Note that the MD simulation is small scale demonstration of the wrapping, which is does not represent the whole surface roughness change, as shown in Figures 1B and C. The microstructure of graphene and PbS-QDs before and after laser shock imprinting was studied using transmission electron microscopy (TEM). As shown in Figure 2A, the graphene/PbS hybrid film after laser shock showed that dense PbS quantum dots (~5 nm) were attached to few layer graphene, and the QDs were tightly sandwiched between two curved graphene films (Figure 2B). The lattice distance of PbS (200) was identified in a graphene+PbS hybrid film after laser shock. In the graphene/QD hybrid film without laser shock imprinting, the attached QD density is much sparser compared to laser shocked situations (Figure 2D). PbS quantum dots were shown only in the two corners of the picture, indicating

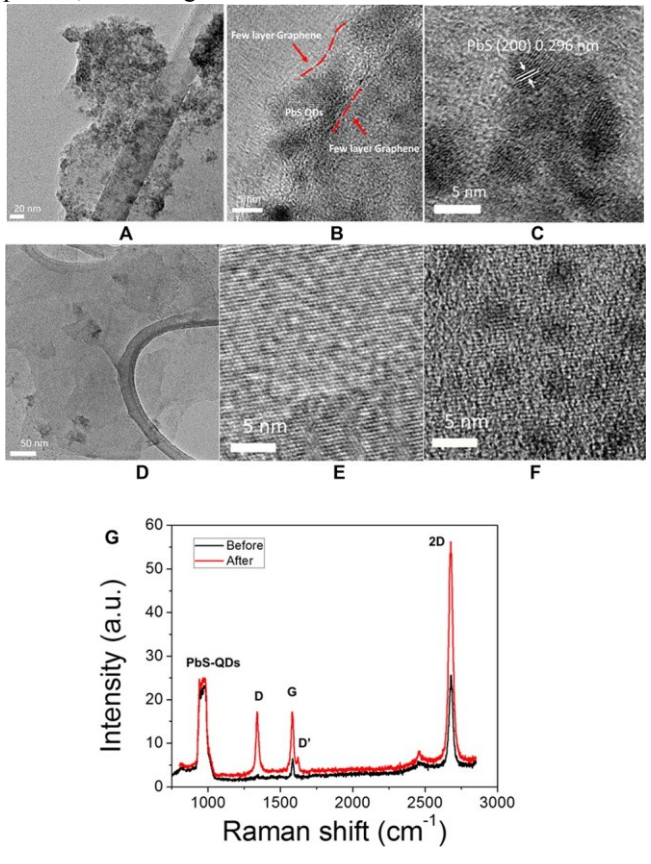

Figure 2. (A) Overview of a fragment of laser shocked graphene+PbS hybrid film under TEM observation. (B) Zoomed TEM image on the edge of the laser shocked graphene+PbS hybrid film. Few layer graphene, marked with red dashed lines, showed a curved shape wrapping around the PbS quantum dots. (C) PbS (200) identified in a graphene+PbS hybrid film after laser shock. (D) Overview of a fragment of graphene+PbS hybrid film without laser shock treatment. (E) Zoomed image at a location where intact graphene was shown. (F) Zoomed image at a location where graphene+PbS is shown, and the graphene lattice is still clear, meaning it was relatively flat. (G) Raman spectra of graphene before and after laser treatment. Laser excitation: 532 nm.

most of the quantum dots were lost during sonication because the attachment was loose. Moreover, the graphene sheets processed by laser shock showed a curved shape, exposing many edge sites (Figure 2B). The graphene sheets that did not undergo laser shock were flat with clear crystal structures (Figure 2E). With a few QDs attached to nonshocked graphene, the crystal structures of graphene were still obvious (see Figure 2F), meaning the graphene hardly deformed there. In shocked graphene/QDs film, crystal structure of graphene can hardly be detected (Figure 2G). In addition, Raman spectra of graphene were collected before and after the process to analyze the effect of laser treatment. As shown in Figure 2G, the rises of the D peak and the D′ peak of graphene are observed after the process, indicating defect generation in the graphene layer induced by laser shock imprinting.

Superior Photodetector Performance with Laser Shock Imprinting of the 2D/0D/2D Structure. To explore effects of the laser shock imprinting on device performance, the I−V curves were measured with light on/off to count response currents. Figure 3 shows the sketches and statistics of photocurrent collected from the graphene/PbS-QDs/graphene photodetectors. As demonstrated in Figure 3A, after GPa scale pressure was applied onto the sandwich structure, it is expected to accomplish tight contact between QDs and graphene. The top layer graphene and PbS-QDs layers are prone to squeezing the bottom layer of graphene, which tends to enhance both the dot−dot contact and dot−graphene interface. The optical image of the fabricated devices is also shown in Figure 3A.

It is well-known that QDs are able to lead to multiphoton emission during solar radiation;[15,16] however, the fluorescence lifetime data on single QD at room temperature reveal that emission is relatively high.[23] According to productive rate equation $G = \alpha N_0 e^{-\alpha x}$ (N_0 is the photon flux at the surface; α is the absorption coefficient, and x is the distance into the material), light intensity exponentially decreases throughout the material. The photogenerated charge is highest at the surface of the material.[24] Although for the nanometer thin QDs layer, we assume light intensity attenuation along depth is neglected. The quantum dot encounters a similar scenario in electron−hole pair excitation and recombination processes under illumination. When multiple electron−hole pairs were excited, they were prone to recombination and light emission unless electron or hole was transferred away. The recombination is the major obstacle of a photodetector because it causes considerable photoexcited carrier loss from signal collection and thereby deteriorates the detector responsivity and detection limit. The top graphene adds another carrier transmission channel, which could efficiently collect photogenerated carrier at the surface of the PbS-QDs layer. The enhanced dot−dot and dot−graphene contacts by laser shock would be able to assist

DOI: 10.1021/acsami.7b14468
ACS Appl. Mater. Interfaces 2017, 11, 44715−44723

electron transport along PbS-QDs layer and the final collection by graphene channel. The enhanced contacts minimize the extended defects over the contact interface, which increases free carrier lifetime and collection possibility. The statement is demonstrated in Figures 3B and C, as drawn from statistical analysis of dozens of devices. The average response current of laser shocked detectors was boosted up for around 2.5 times with gate voltage of both 5 V (from ~0.4 to ~1.0 μA) and 20 V (from ~20 to ~50 μA), resulting from more efficient exciton collection. Note that the considerable error bar before/after laser shock imprinting is due to variations in performance among devices. The deviation of performance originated from complex factors during device fabrication such as graphene electrode size, wet transferring, and device lithography and metallization.

Figure 4 illustrates the specific on/off performance of one sandwich structure photodetector before and after the laser shock process. As shown in Figure 4A, before laser shock, the photocurrent is 58.2 μA, while the dark current is 58.7 μA; therefore, the response current was calculated as 0.5 μA at the gate voltage of 5 V. When compared side by side in Figure 4A, the photocurrent achieves 56.2 μA, and the dark current is 57.1 μA, which accounts for the response current of 0.9 μA. The apparently stronger response current signal was accomplished due to more efficient carrier collection and transportation. Figure 4B illustrates the same device performance with higher gate voltage of 20 V; the response current increases to 30.5 μA after laser shock from 18 μA before laser shock. After laser shock, the dark current is 2.5 μA, and the photocurrent is 33.0 μA. This indicates higher potential along gate could enhance the on/off (I_d/I_p) ratio from 1.8 to 13.2, which is the best in all reported graphene hybrid photodetectors, as summarized in Table 1. As demonstrated by a comparison of before and after laser shock, to more thoroughly understand the photodetector performance, the photo responsivity was calculated with known incident light source. As described in the Experimental Section, an LED light source in wavelength of 650 nm and intensity of 430 μW/cm^2 was utilized. Because adjacent electrodes are spaced in the range of 200 μm, the corresponding incident light intensity per detector was drawn to be 0.86 μW; thereby, the detector responsivity was conducted as 58 A/W after laser shock comparing to 22 A/W before. Not only did response current increase by three times after laser shock, but the on/off response speed also increased, as shown in Figures 4A and 3B. The plots, especially the curve switching light on and off in Figures 4C and D (distant between red dot lines and black dot lines), apparently denote a slow switch for photocurrent with a lifting time before laser shock and a sharp switch within an ultrashort time after laser shock. The lifting time is around 0.6 s (both 5 V gate and 20 V gate) for the detector to reach maximum photocurrent before laser

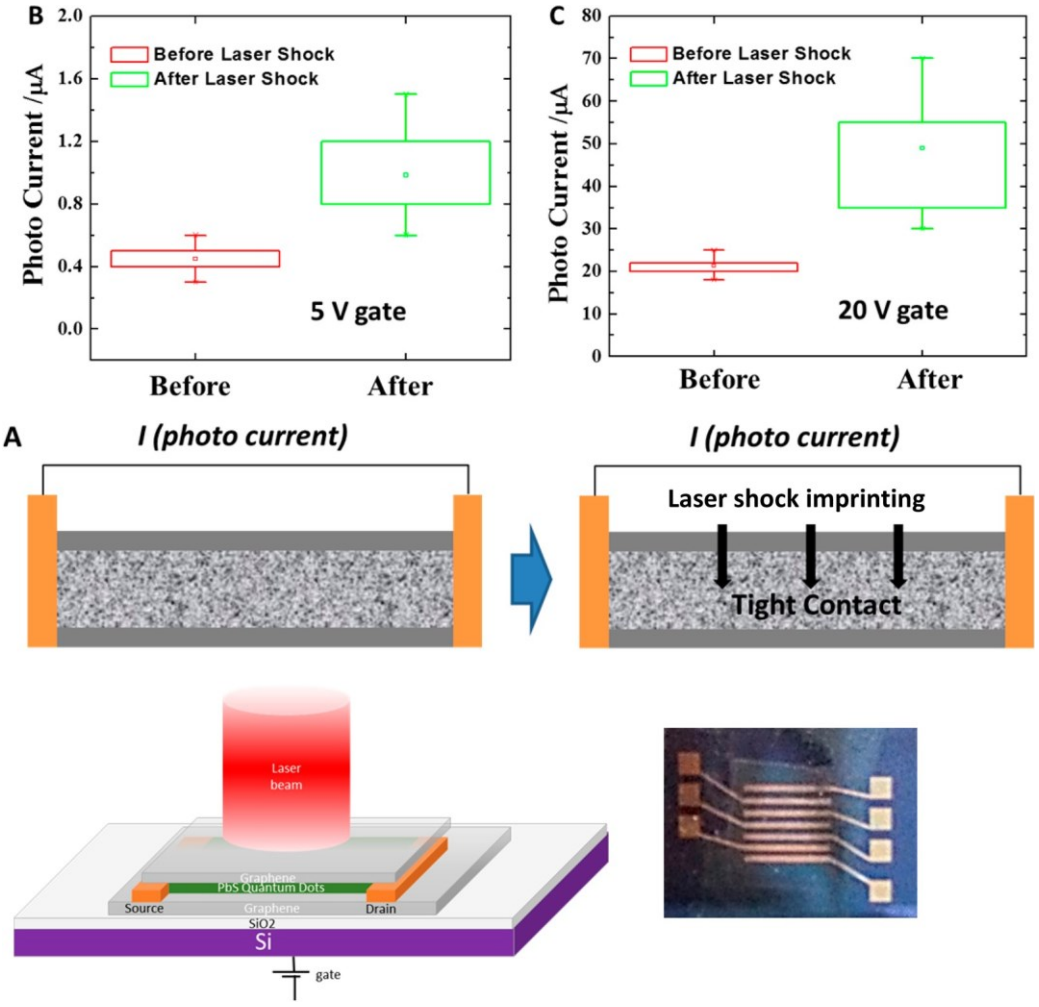

Figure 3. Performance of graphene/PbS/graphene photodetectors. (A) Structures of graphene/PbS-QDs/graphene photodetectors before and after laser shock. (B) and C) Box chart of photocurrent collected by hybrid photodetectors of graphene wrapped PbS-QDs before and after laser shock fabrication at the gate voltage of 5 and 20 V.

DOI: 10.1021/acsami.7b14468
ACS Appl. Mater. Interfaces 2017, 9, 44715−44721

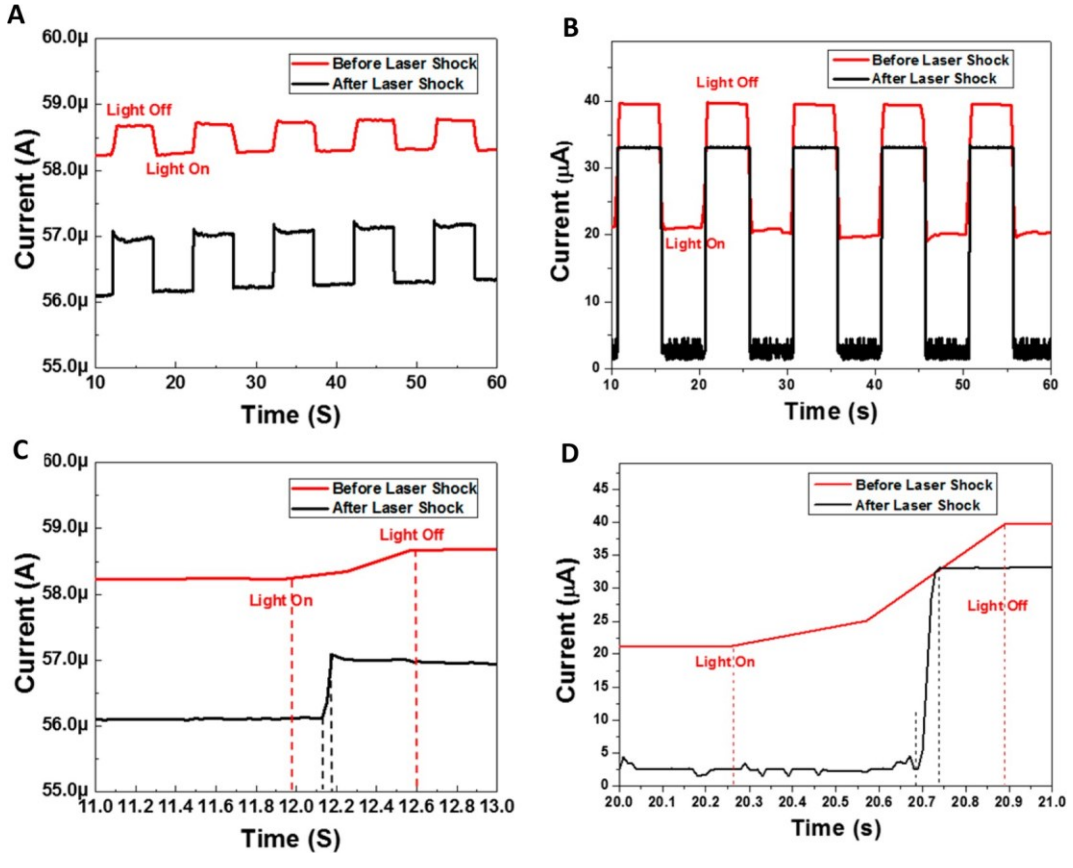

Figure 4. Transient response of graphene/PbS/graphene photodetector. (A and B) I−t curve of graphene/PbS/graphene hybrid photosensor before and after the laser shock process at the gate voltage of 5 and 20 V. (C and D) Magnified image for photocurrent of the I−t curve: graphene/PbS/ graphene hybrid photosensor before and after laser shock under gate voltage of 5 and 20 V.

shock, which is faster than that of PbS-QDs/graphene device on account of the encapsulation and conduction of the top graphene. However, it can be compared afterward, the lifting time for switching light on and off become less than 0.05 s (~0.05 s for 5 V gate and ~0.03 s for 20 V gate). These significant enhancements of response gain, on/off ratio, responsivity, and lifting time indicate that the free carrier transferring process[25] was dramatically boosted after laser shock.

Mechanism of Optomechanical Integration of Graphene with PbS-QDs. The effect of laser shock imprinting on wrapping of graphene on PbS-QDs was further revealed by molecular dynamics (MD) simulation. The dot diameter was 8 nm, and the interparticle distance was 12 nm. Bond−bond interaction between carbon atoms of graphene was described by adaptive intermolecular reactive empirical bond order (AIREBO) potential with a cutoff distance 2.0 Å. Lennard−Jones (LJ) potential was used for particle−graphene interaction: $\varepsilon c - np = 0.89$ meV, $\sigma c - np = 3.629$ Å. The van der Waals (vdW) interaction between graphene and the substrate was modeled by using the same potential with parameters. The system was calculated in ensemble NVT (Nose−Hoover thermostat) with the temperature maintained at 300 K. The time step was 1 fs. In Figure 1D, before laser shock, the graphene was suspended on the top of asperous QDs surface. After laser shock was applied to the multilayer structure, as shown in Figure 1E, graphene was tightly contacted with the QDs layer underneath due to the 10 GPa scale mechanical pressure. The tight contact between graphene electrode and QDs layer increased the free carrier transferring process between them. The simulation results are consistent with the AFM measurement before and after laser shock imprinting (Figures 1B and C).

Table 1. Performance of Graphene Hybrid Photodetectors

ref	V_g (V)	light power density	I_p/I_d ratio	response time
PbS/G[17]	−20 to 80	6.68 mW/cm^2	<1.1	not given
PbS/G[16]	−40 to 60	~0.5 mW/cm^2	<2	~2 s
PbS/G[15]	30 to 60	32.7 mV/cm^2		5 s
PbS/G[26]	−10	not given	[redacted].03	not given
perovskite/G[27]	−80 to 90	1 mW/cm^2	<1.5	0.54 s
G/PbS/G	20	0.43 mW/cm^2	~1.8	~0.65 s
G/PbS/G	20	0.43 mW/cm^2	~13	~50 ms

Optical properties of the hybrid thin film were studied to understand the effects laser shock imprinting on the interfaces between the graphene/PbS/graphene layers and the glass substrate. As shown in Figure 5A, a single layer of graphene was transferred onto the glass slide for the control experiment. Lambda 950 was used to collect film

DOI: 10.1021/acsami.7b14468
ACS Appl. Mater. Interfaces 2017, 11, 44715−44723

transmittance as a function of increasing wavelength from 400 to 1600 nm. The sample film was stabilized between the lambda 950 light source and integrating sphere so that the incident light intensity and light intensity after film absorption could be compared. In Figure 5A, full-wave higher light transmittance is displayed after laser shock, implying laser shock induced pressure can enhance the contact between the graphene layer and the glass substrate underneath. The enhanced contact is because laser shock imprinting can reduce graphene wrinkles and ridges, as shown in the AFM images before and after laser shock imprinting (Figures 1B and C). Graphene wrapped by QDs and sole PbS QDs layers was also investigated by light transmittance measurements. In Figure 5B, sole PbS layer shows a very small significant transmittance change before and after laser shock. However, a significant light transmittance increase is shown in Figure 5B for graphene wrapped by a QDs layer after laser shock imprinting, which indicates similar contact improvement by laser shock.

Mechanism of Carrier Transfer between Graphene and PbS-QDs. We further measured the graphene/PbS-QDs/graphene device after laser shock in detail to reveal the reason for negative response at positive gate voltages and the mechanism of carrier transfer between graphene and PbS QDs. Figure 6A shows transfer curves of the device from −5 to 5 V in dark state and under illumination, describing the typical p-type characteristic and no photoresponse at negative gate voltage. The transfer curves are enlarged from 0 to 10 V in Figure 6B, which displays very weak positive response before 4.2 V gate and very strong negative response after 4.2 V gate to the same light source. A sharp decrease in current begins around 4.2 V gate, which is due to band structure evolution and charge transmission of our device by gate voltage. In other PbSQDs/graphene hybrid systems,[15−17,28] the carrier transfer from PbS-QDs to graphene was elaborated as electrons or holes dominated. Our opinion is that whether electrons or holes dominate the carrier transfer is due to the band structure, which is also proposed in recent studies.[26,29,30] Along with photoexcitation and gate voltage modulation, the carrier density

DOI: 10.1021/acsami.7b14468
ACS Appl. Mater. Interfaces 2017, 11, 44715−44723

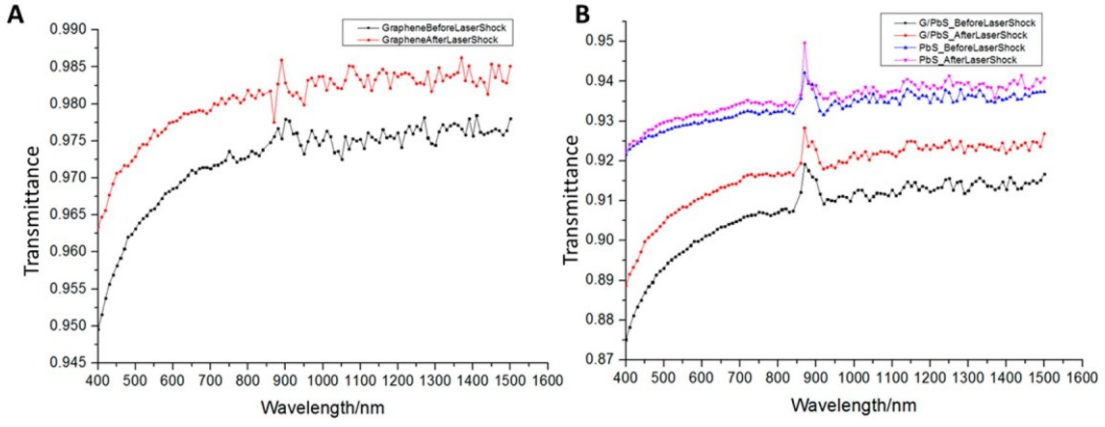

Figure 5. Transmittance of graphene/PbS-QDs/graphene multilayer. (A) Transmittance of single layer graphene on substrate as a function of wavelength before and after the laser shock process. (B) Transmittance of single layer QDs film and graphene/QDs multilayer on substrate as a function of wavelength before and after the laser shock process.

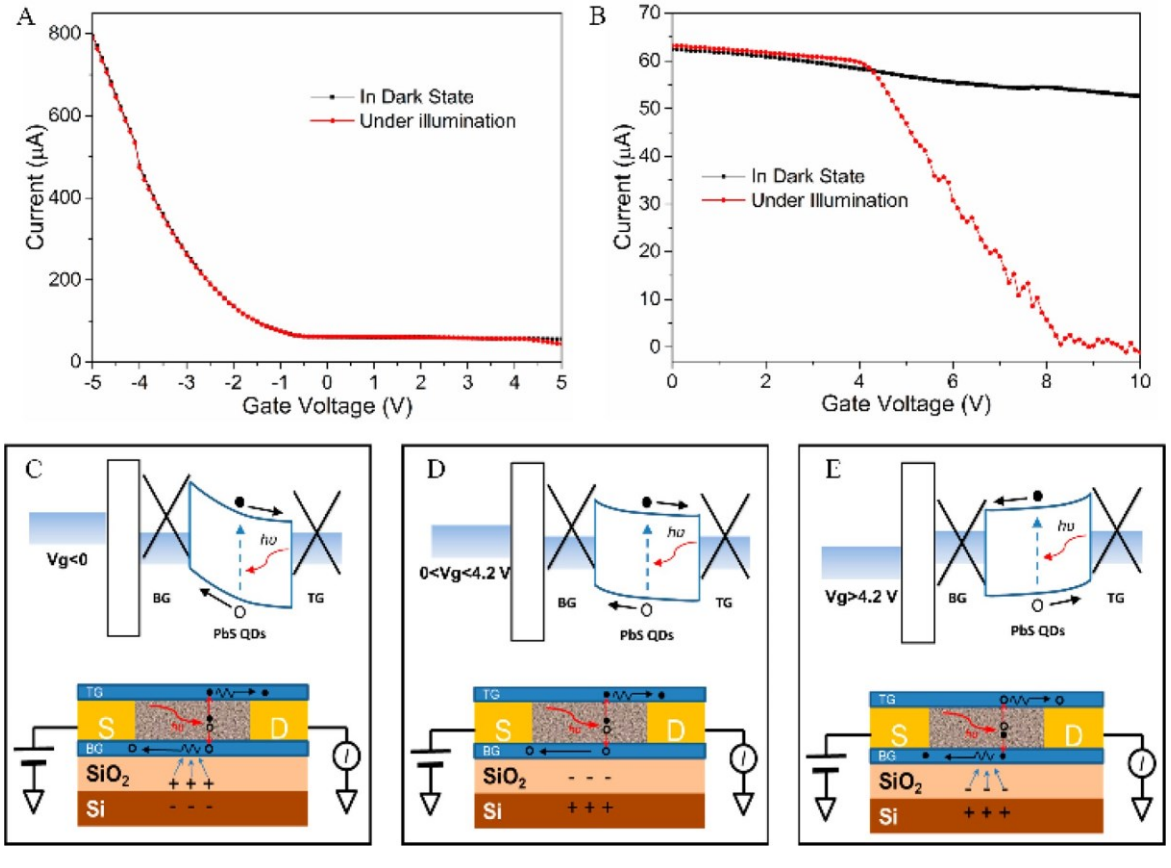

Figure 6. Transfer curves of the device and band structure evolution of graphene/PbS QDs/graphene heterojunction. (A and B) Transfer curves in different gate voltage ranges. The drain−source voltage is 10 mV. The light source is 430 μW/cm^2 at 650 nm. (C−E) Band structure evolutions and charge transmission at different gate voltages. TG and B mean top graphene and bottom graphene, respectively.

changes in PbS-QDs and graphene make the band structure rebalance, which decides the dynamic carrier transfer from PbSQDs to graphene.[26]

To explain the back-gate modulation on photoresponse of our graphene/PbS-QDs/graphene device, the band structure evolutions and charge transmission at $V_g < 0$, $0 < V_g < 4.2$ V, and $V_g > 4.2$ V are shown in Figures 6C−E. There are two synergistic mechanisms for photoconductivity in the graphene/ PbS-QDs/graphene device: the photogenerated carrier injection from PbS-QDs to top graphene and bottom graphene (equivalent to carrier density), and the charge transmission in top graphene and bottom graphene (equivalent to carrier mobility). The transfer curves in Figure 6A indicate the whole device is weakly p-type and of hole transport due to a p-type doping effect on the bottom graphene by the substrate oxide.[31] The Fermi level of EDT-passivated PbS-QDs is closer to the valence band,[32] and the work function is about 4.7−4.9 eV.[33,34] With the finite density

DOI: 10.1021/acsami.7b14468
ACS Appl. Mater. Interfaces 2017, 11, 44715−44723

of state and weak electrostatic screening of graphene,[6,35,36] the interface between bottom graphene and PbS-QDs can be effectively modulated by back-gate voltage. At negative gate voltage, the work function of bottom graphene shifts up[37] to form photogenerated hole injection to bottom graphene and photogenerated electron injection to top graphene, as displayed in Figure 6C. The negative gate induces the weak substrate scattering to holes in the p-type bottom graphene channel, and the surface adsorbates scatter the electron transportation in top graphene,[38] leading to worse charge transmission, which neutralizes improvement of photoresponse by carrier injection. As a result, our device shows very weak positive or even no photoresponse at negative gate voltage in Figure 6A and Figure 7. Along the back gate

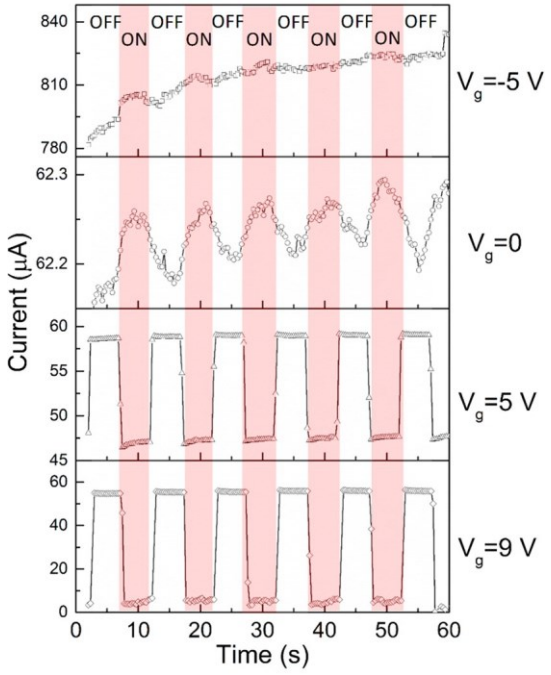

Figure 7. Transient response of the graphene/PbS QDs/graphene device at different gate voltages.

increases to positive (Figure 6D), the hole injection to bottom graphene decreases, but the gate-induced substrate scattering disappears, leading to stronger positive photoresponse in Figure 6B and Figure 7. When the gate voltage is over 4.2 V (Figure 6E), we could deduce that the work function of bottom graphene further shifts down to form electron injection to bottom graphene and hole injection to top graphene.[37] The strong positive gate induces strong substrate scattering to electrons in the bottom graphene and the surface adsorbates scatter holes in the top graphene,[38] leading to much worse charge transmission and negative photoresponse, as shown in Figure 6B and Figure 7. Along with the increase in gate voltage, the negative photoresponse becomes stronger. These photoresponse phenomena are quite reproducible as the yield of working devices is very high (at least 45 working devices out of 60 original graphene/PbS QDs/graphene devices).

We further measured the performance of graphene/PbS/graphene. The light power density dependent response is shown in Figure 8A. Under $<10^{-5}$ W/cm^2 power density incidence, the response current, as calculated as absolute difference between dark and photocurrent, increases linearly along the incident power. The linear dynamic range (LDR) is over four orders of magnitude. The response saturation under strong irradiance is attributed to the gradual filling of high-gain deep defects along with the increase in incident light intensity.[39,40] Figure 8B displays wavelength dependent responsivity. The responsivity (R) is calculated by the equation

$$R = \frac{|I_p - I_d|}{P_{in}}$$

where I_p is the photocurrent, I_d is the dark current, and P_{in} is the incident power. The wavelength dependent responsivity is consistent with the absorption of PbS QDs film. The responsivity to shorter wavelength light is a little higher than longer wavelength light. There is a responsivity peak around 1050 nm, corresponding the exciton absorption peak. The detectivity (D*) is calculated by the equation

$$D^* = \frac{R\sqrt{A}}{\sqrt{2qI_d}}$$

where R is the responsivity, A is the active area of the device, and q is the electron charge. The responsivity is over 10 A/W, and the detectivity reaches 2×10^{11} Jones at the gate voltage of 10 V. An obvious valley at $V_g = 4.2$ V is attributed to the modulation of gate voltage on the carrier injection from PbS QDs to graphene (Figure 6).

CONCLUSION

In this work, we reported a cost-efficient, scalable laser shock imprinting method that was used to manipulate the interface between 2D and 0D materials. The laser shock method tuned morphology of 2D materials on 0D materials to perfect wrapping rather than grid-space contact. The wrapping of PbSQDs with graphene can enhance the transmission, photoresponse gain, and photoresponse speed of photodetectors. Surface morphology investigation, response current under gate voltage, optical transmittance, and physical simulation confirm our statement. The photoresponse gain increases by 2×; the photoresponse speed of photodetectors raises by over 13×, and response time reduces by 20× after laser shock wrapping of the laminates. The response time ~30 ms after laser shock is the shortest, and the I_p/I_d ratio ~13 is highest in all reported graphene hybrid photodetectors. This is due to the tight

DOI: 10.1021/acsami.7b14468
ACS Appl. Mater. Interfaces 2017, 11, 44715−44723

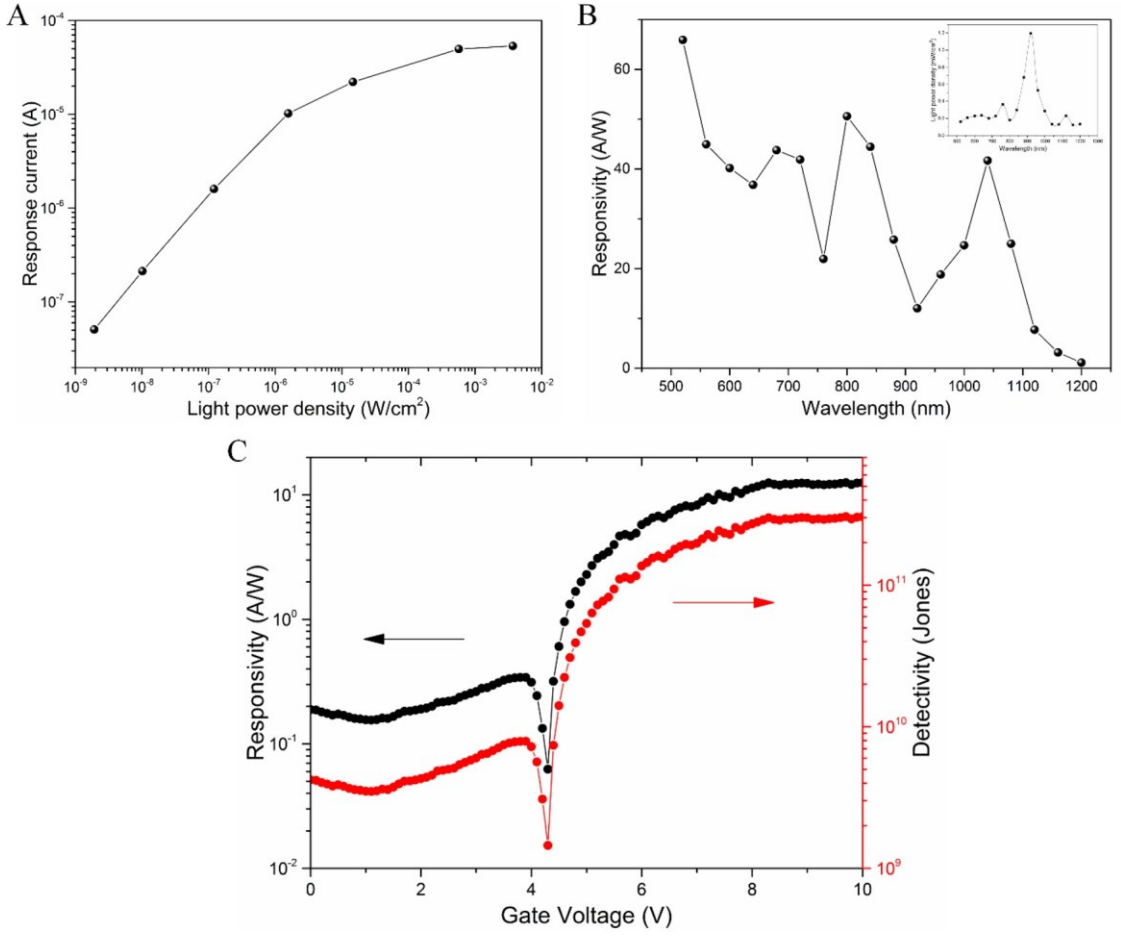

Figure 8. Performance of graphene/PbS/graphene photodetector at gate voltage of 20 V and drain-source bias of 1 V. (A) 650 nm light power density dependent response. The response current means the absolute difference between dark and photocurrent. (B) Wavelength dependent responsivity. The monochromatic source is a xenon lamp modulated by grating with a frequency of 20 Hz. The inset shows light power density. (C) Responsivity and detectivity as a function of gate voltage illuminated by 650 nm light with a power density of 430 μW/cm^2.

contact between PbS-QDs and graphene after laser shock and more efficient gate-modulated carrier injection from PbS-QDs to graphene. Through the careful deduction of band structure change, we found gate voltage dictates whether electrons or holes dominate the carrier injection from PbS QDs to graphene, corresponding to different photoresponses.

EXPERIMENT METHODS

Device Fabrication. PbS-QDs were synthesized and isolated according to a modified Hines method. The oleic acid-passivated PbSQDs were dispersed in toluene at a concentration of 50 mg/mL. Single layer CVD graphene was transferred onto a Si/SiO_2 (285 nm) wafer. Patterned using a designed mask on the top of the graphene, Au (50 nm)/Ti (5 nm) source and drain electrodes were deposited by thermal evaporation. The PbS-QDs in toluene were deposited onto graphene by spin-coating and treated by ethanedithiol (EDT) method. This process was repeated three times. Afterward, the graphene/PbS QDs device was baked at 90 °C in air for 10 min. Another single layer CVD graphene was transferred onto the PbS-QDs film. Finally, laser shock imprinting was used to fabricate the device.

Laser Shock Imprinting. Nd:YAG (Continuum Surelite III) was used as the energy source. The laser beam was set to be 4 mm in diameter with 10 ns as pulse width. A carbon coated aluminum foil covered the top of the samples. A transparent confinement glass layer was covered tightly on top of the carbon coated aluminum foil.

TEM Sample Preparation. The laser shocked and nonshocked graphene/PbS QD hybrid structures were first prepared on flat substrates. A small drop of ethanol was dropped on the hybrid location followed by a TEM grid covering on top. As the ethanol droplet dried, we applied tweezer tips to slowly glide the TEM grid around the sample location. Friction between the TEM grid and the substrate transferred fragments of graphene/PbS hybrid onto the grid for final TEM observation.

Optoelectronic Characterizations. All characterizations of device performance were done in an optically and electrically sealed box to minimize electromagnetic disturbance. The monochromatic light source for photoresponse testing was a 650 nm LED modulated by a waveform generator (Agilent 33600A Series). Transient photoresponse and transfer curves were measured using a semiconductor device analyzer (Agilent B1500A) by averaging the current over time for each voltage step.

DOI: 10.1021/acsami.7b14468
ACS Appl. Mater. Interfaces 2017, 11, 44715−44723

AUTHOR INFORMATION

Corresponding Authors *E-mail: gjcheng@purdue.edu.

*E-mail: jtang@mail.hust.edu.cn.

ORCID

Jiang Tang: 0000-0003-2574-2943

Gary J. Cheng: 0000-0002-1184-2946

Notes

The authors declare no competing financial interest.

ACKNOWLEDGMENTS

We sincerely thank financial support from the United States National Science Foundation through CMMI (Grant 1538360) and the Purdue SMART Consortium and Office of Naval research through the DURIP program.

REFERENCES

(1) Yang, W.; Chen, G.; Shi, Z.; Liu, C.-C.; Zhang, L.; Xie, G.; Cheng, M.; Wang, D.; Yang, R.; Shi, D. Epitaxial growth of singledomain graphene on hexagonal boron nitride. Nat. Mater. 2013, 12, 792−797.

(2) Grosse, K. L.; Bae, M.-H.; Lian, F.; Pop, E.; King, W. P. Peltier cooling and current crowding at graphene−metal contacts. Nat. Nanotechnol. 2011, 6, 287−290.

(3) Xia, F.; Perebeinos, V.; Lin, Y.-m.; Wu, Y.; Avouris, P. The origins and limits of metal−graphene junction resistance. Nat. Nanotechnol. 2011, 6, 179−184.

(4) Venugopal, A.; Colombo, L.; Vogel, E. Contact resistance in few and multilayer graphene devices. Appl. Phys. Lett. 2010, 96, 013512.

(5) Britnell, L.; Gorbachev, R.; Geim, A.; Ponomarenko, L.; Mishchenko, A.; Greenaway, M.; Fromhold, T.; Novoselov, K.; Eaves, L. Resonant tunnelling and negative differential conductance in graphene transistors. Nat. Commun. 2013, 4, 1794.

(6) Britnell, L.; Gorbachev, R.; Jalil, R.; Belle, B.; Schedin, F.; Mishchenko, A.; Georgiou, T.; Katsnelson, M.; Eaves, L.; Morozov, S. Field-effect tunneling transistor based on vertical graphene heterostructures. Science 2012, 335, 947−950.

(7) Geringer, V.; Liebmann, M.; Echtermeyer, T.; Runte, S.; Schmidt, M.; Rückamp, R.; Lemme, M. C.; Morgenstern, M. Intrinsic and extrinsic corrugation of monolayer graphene deposited on SiO2. Phys. Rev. Lett. 2009, 102, 076102.

(8) Geim, A. K.; Novoselov, K. S. The rise of graphene. Nat. Mater. 2007, 6, 183−191.

(9) Bonaccorso, F.; Sun, Z.; Hasan, T.; Ferrari, A. Graphene photonics and optoelectronics. Nat. Photonics 2010, 4, 611−622.

(10) Dean, C. R.; Young, A. F.; Meric, I.; Lee, C.; Wang, L.; Sorgenfrei, S.; Watanabe, K.; Taniguchi, T.; Kim, P.; Shepard, K. Boron nitride substrates for high-quality graphene electronics. Nat. Nanotechnol. 2010, 5, 722−726.

(11) Geim, A. K. Graphene: status and prospects. Science 2009, 324, 1530−1534.

(12) Roy, K.; Padmanabhan, M.; Goswami, S.; Sai, T. P.; Ramalingam, G.; Raghavan, S.; Ghosh, A. Graphene-MoS2 hybrid structures for multifunctional photoresponsive memory devices. Nat. Nanotechnol. 2013, 8, 826−830.

(13) Shi, G.; Hanlumyuang, Y.; Liu, Z.; Gong, Y.; Gao, W.; Li, B.; Kono, J.; Lou, J.; Vajtai, R.; Sharma, P. Boron nitride-graphene nanocapacitor and the origins of anomalous size-dependent increase in capacitance. Nano Lett. 2014, 14, 1739−1744.

(14) Wang, X.; Zhi, L.; Müllen, K. Transparent, conductive graphene electrodes for dye-sensitized solar cells. Nano Lett. 2008, 8, 323−327. (15) Sun, Z.; Liu, Z.; Li, J.; Tai, G. a.; Lau, S. P.; Yan, F. Infrared photodetectors based on CVD-grown graphene and PbS quantum dots with ultrahigh responsivity. Adv. Mater. 2012, 24, 5878−5883.

(16) Konstantatos, G.; Badioli, M.; Gaudreau, L.; Osmond, J.; Bernechea, M.; de Arquer, F. P. G.; Gatti, F.; Koppens, F. H. Hybrid graphene-quantum dot phototransistors with ultrahigh gain. Nat. Nanotechnol. 2012, 7, 363−368.

(17) Zhang, D.; Gan, L.; Cao, Y.; Wang, Q.; Qi, L.; Guo, X. Understanding charge transfer at PbS-decorated graphene surfaces toward a tunable photosensor. Adv. Mater. 2012, 24, 2715−2720.

(18) Li, X.; Zhu, Y.; Cai, W.; Borysiak, M.; Han, B.; Chen, D.; Piner, R. D.; Colombo, L.; Ruoff, R. S. Transfer of large-area graphene films for high-performance transparent conductive electrodes. Nano Lett. 2009, 9, 4359−4363.

(19) Fabbro, R.; Fournier, J.; Ballard, P.; Devaux, D.; Virmont, J. J. Physical study of laser-produced plasma in confined geometry. J. Appl. Phys. 1990, 68, 775−784.

(20) Gao, H.; Hu, Y.; Xuan, Y.; Li, J.; Yang, Y.; Martinez, R. V.; Li, C.; Luo, J.; Qi, M.; Cheng, G. J. Large-scale nanoshaping of ultrasmooth 3D crystalline metallic structures. Science 2014, 346, 1352−1356.

(21) Li, J.; Liao, Y.; Suslov, S.; Cheng, G. J. Laser shock-based platform for controllable forming of nanowires. Nano Lett. 2012, 12, 3224−3230.

(22) Kim, C. O.; Hwang, S. W.; Kim, S.; Shin, D. H.; Kang, S. S.; Kim, J. M.; Jang, C. W.; Kim, J. H.; Lee, K. W.; Choi, S. H.; Hwang, E. High-performance graphene-quantum-dot photodetectors. Sci. Rep. 2015, 4, 5603.

(23) Das, S. R.; Nian, Q.; Saei, M.; Jin, S.; Back, D.; Kumar, P.; Janes, D. B.; Alam, M. A.; Cheng, G. J. Single-Layer Graphene as a Barrier Layer for Intense UV Laser-Induced Damages for Silver Nanowire Network. ACS Nano 2015, 9, 11121−11133.

(24) Tabak, M. D.; Warter, P. J., Jr Transition from Emission-Limited to Space-Charge-Limited Photoconductivity. Phys. Rev. 1968, 173, 899.

(25) Nian, Q.; Zhang, M. Y.; Wang, Y.; Das, S. R.; Bhat, V. S.; Huang, F.; Cheng, G. J. Charge carrier transport and collection enhancement of copper indium diselenide photoactive nanoparticle-ink by laser crystallization. Appl. Phys. Lett. 2014, 105, 111909.

(26) Huang, Y.; Zhu, R.; Kang, N.; Du, J.; Xu, H. Photoelectrical response of hybrid graphene−PbS quantum dot devices. Appl. Phys. Lett. 2013, 103, 143119.

(27) Lee, Y.; Kwon, J.; Hwang, E.; Ra, C. H.; Yoo, W. J.; Ahn, J. H.; Park, J. H.; Cho, J. H. High-performance perovskite-graphene hybrid photodetector. Adv. Mater. 2015, 27, 41−46.

(28) Gao, L.; Dong, D.; He, J.; Qiao, K.; Cao, F.; Li, M.; Liu, H.; Cheng, Y.; Tang, J.; Song, H. Wearable and sensitive heart-rate

DOI: 10.1021/acsami.7b14468
ACS Appl. Mater. Interfaces 2017, 11, 44715−44723

detectors based on PbS quantum dot and multiwalled carbon nanotube blend film. Appl. Phys. Lett. 2014, 105, 153702.
(29) Hu, L.; Li, D. B.; Gao, L.; Tan, H.; Chen, C.; Li, K.; Li, M.; Han, J. B.; Song, H.; Liu, H. Graphene Doping Improved Device Performance of ZnMgO/PbS Colloidal Quantum Dot Photovoltaics. Adv. Funct. Mater. 2016, 26, 1899−1907.
(30) Gao, L.; Chen, C.; Zeng, K.; Ge, C.; Yang, D.; Song, H.; Tang, J. Broadband, sensitive and spectrally distinctive SnS2 nanosheet/PbS colloidal quantum dot hybrid photodetector. Light: Sci. Appl. 2016, 5, e16126.
(31) Ryu, S.; Liu, L.; Berciaud, S.; Yu, Y.-J.; Liu, H.; Kim, P.; Flynn, G. W.; Brus, L. E. Atmospheric oxygen binding and hole doping in deformed graphene on a SiO_2 substrate. Nano Lett. 2010, 10, 4944− 4951.
(32) Chuang, C.-H. M.; Brown, P. R.; Bulovic, V.; Bawendi, M. G̀. Improved performance and stability in quantum dot solar cells through band alignment engineering. Nat. Mater. 2014, 13, 796.
(33) Pang, S.; Tsao, H. N.; Feng, X.; Müllen, K. Patterned Graphene Electrodes from Solution-Processed Graphite Oxide Films for Organic Field-Effect Transistors. Adv. Mater. 2009, 21, 3488−3491.
(34) Cao, Y.; Wei, Z.; Liu, S.; Gan, L.; Guo, X.; Xu, W.; Steigerwald, M. L.; Liu, Z.; Zhu, D. High-performance Langmuir-Blodgett monolayer transistors with high responsivity. Angew. Chem. 2010, 122, 6463−6467.
(35) Yang, H.; Heo, J.; Park, S.; Song, H. J.; Seo, D. H.; Byun, K.-E.; Kim, P.; Yoo, I.; Chung, H.-J.; Kim, K. Graphene barristor, a triode device with a gate-controlled Schottky barrier. Science 2012, 336, 1140−1143.
(36) Yu, W. J.; Li, Z.; Zhou, H.; Chen, Y.; Wang, Y.; Huang, Y.; Duan, X. Vertically stacked multi-heterostructures of layered materials for logic transistors and complementary inverters. Nat. Mater. 2012, 12, 246.
(37) Yu, W. J.; Liu, Y.; Zhou, H.; Yin, A.; Li, Z.; Huang, Y.; Duan, X. Highly efficient gate-tunable photocurrent generation in vertical heterostructures of layered materials. Nat. Nanotechnol. 2013, 8, 952−958.
(38) Biswas, C.; Günes, F.; Loc, D. D.; Lim, S. C.; Jeong, M. S.; Pribat, D.; Lee, Y. H. Negative and Positive Persistent Photoconductance in Graphene. Nano Lett. 2011, 11, 4682−4687.
(39) Greenham, N. C.; Peng, X.; Alivisatos, A. P. Charge separation and transport in conjugated-polymer/semiconductor-nanocrystal composites studied by photoluminescence quenching and photoconductivity. Phys. Rev. B: Condens. Matter Mater. Phys. 1996, 54, 17628.
(40) McDonald, S. A.; Konstantatos, G.; Zhang, S.; Cyr, P. W.; Klem, E. J.; Levina, L.; Sargent, E. H. Solution-processed PbS quantum dot infrared photodetectors and photovoltaics. Nat. Mater. 2005, 4, 138− 142.

DOI: 10.1021/acsami.7b14468
ACS Appl. Mater. Interfaces 2017, 11, 44715−44723